Inorganic Chemistry

Article

pubs.acs.org/IC

Influence of Halogen Atoms on a Homologous Series of Bis-Cyclometalated Iridium(III) Complexes

Etienne Baranoff,*[,†] Basile F. E. Curchod,[‡] Filippo Monti,[§] Frédéric Steimer,[‡] Gianluca Accorsi,*[,§] Ivano Tavernelli,[‡] Ursula Rothlisberger,[‡] Rosario Scopelliti,[†] Michael Grätzel,[†] and Md. Khaja Nazeeruddin[†]

[†]Laboratory of Photonics and Interfaces and [‡]Laboratory of Computational Chemistry and Biochemistry, Institute of Chemical Sciences and Engineering, School of Basic Sciences, École Polytechnique Fédérale de Lausanne, CH-1015 Lausanne, Switzerland

[§]Molecular Photoscience Group, Istituto per la Sintesi Organica e la Fotoreattività, Consiglio Nazionale delle Ricerche, Via P. Gobetti 101, 40129, Bologna, Italy

Supporting Information

ABSTRACT: A series of homologous bis-cyclometalated iridium(III) complexes Ir(2,4-di-X-phenyl-pyridine)$_2$-(picolinate) (X = H, F, Cl, Br) **HIrPic**, **FIrPic**, **ClIrPic**, and **BrIrPic** has been synthesized and characterized by NMR, X-ray crystallography, UV−vis absorption and emission spectroscopy, and electrochemical methods. The addition of halogen substituents results in the emission being localized on the main cyclometalated ligand. In addition, halogen substitution induces a blue shift of the emission maxima, especially in the case of the fluoro-based analogue but less pronounced for chlorine and bromine substituents. Supported by ground and excited state theoretical calculations, we rationalized this effect in a simple manner by taking into account the σp and σm Hammett constants on both the highest occupied molecular orbital (HOMO) and the lowest unoccupied molecular orbital (LUMO) energy levels. Furthermore, in comparison with **FIrPic** and **ClIrPic**, the impact of the large bromine atom remarkably decreases the photoluminescence quantum yield of **BrIrPic** and switches the corresponding lifetime from mono to biexponential decay. We performed theoretical calculations based on linear-response time-dependent density functional theory (LR-TDDFT) including spin−orbit coupling (SOC), and unrestricted DFT (U-DFT) to obtain information about the absorption and emission processes and to gain insight into the reasons behind this remarkable change in photophysical properties along the homologous series of complexes. According to theoretical geometries for the lowest triplet state, the large halogen substituents contribute to sizable distortions of specific phenylpyridine ligands for **ClIrPic** and **BrIrPic**, which are likely to play a role in the emissive and nonradiative properties when coupled with the heavy-atom effect.

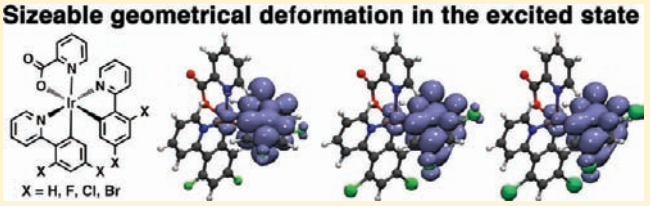

INTRODUCTION

Photochemistry and photophysics of transition metal complexes continue to attract interest in particular because of their relevant practical applications for solving energy issues.[1] Alteration of the excited-state properties of the transition metal complexes through systematic chemical modification of the ligands resulted over decades in enormous number of photoactive molecules.[2,3] General design rules have been derived from these results, and it is nowadays relatively straightforward to predict and therefore to adjust at will any given property of transition-metal complexes such as redox potentials, emission or absorption maximum wavelength, or quantum yield of photoinduced processes. However, because of the close interplay of all these properties, the difficulty is to control all these aspects at once and obtain fully optimized materials with desired properties. In this respect, the accurate understanding of structure-properties relationships[4,5] is highly sought after.[6] Since very few parameters are modified, preferably one only, the study of homologous series are of fundamental interest to unequivocably understand the effect of a specific chemical or structural change on the sample properties. This is because the properties of molecules are expected to vary in a systematic way with their chemical structure. Hammett parameters have been highly successful as a structural parameter which can be related to chemical and physical properties of the molecules.[7] While the Hammett equation[8] has been initially used for gaining insight into chemical reactions and their mechanism, Hammett parameters are very powerful to correlate chemical structures to electronic properties such as redox potentials[9] and absorption and emission maxima.[10] Besides inductive and resonance effects, another influence of substituents on photophysical properties of organic molecules is through the heavy atom effect, which enhances the rate of spin-forbidden processes. In this case, halogen-based homologous series have been classically used.[11] On the other hand, the effect of halogen substituents on organometallic complexes has not been investigated as much as in the case of organic chromophores. As being part of the same family of

Received: May 29, 2011
Published: December 22, 2011

substituents, we believe that homologous series based on halogen substituents are of particular interest to improve the understanding of photophysical processes in transition metal complexes.

Because of their high photoluminescence quantum yields (PLQY), wide color tunability, relatively short excited-state lifetime, and general thermal and electrochemical stability, cyclometalated iridium(III)[12−15] complexes are attracting widespread interest for a large range of luminescence-based applications.[16] Chlorine and bromine atoms have been used as substituents for charged complexes.[17] In these complexes, the triplet levels are known to be localized on the N^N ancillary ligand when bipyridine or phenanthroline units are also involved in the metal core complexation.[18] Therefore the substituents on the main ligands affect primarily the highest occupied molecular orbital (HOMO) of the complex without significant impact on the lowest unoccupied molecular orbital (LUMO). Limited studies exist on neutral cyclometalated iridium complexes with bromine as substituents[19,20] and none using chlorine.

Here, we report the results on a homologous neutral series of biscyclometalated iridium(III) complexes Ir(2,4-di-X-phenylpyridine)$_2$(picolinate) (X = H, F, Cl, Br). Data for the nonsubstituted complex **HIrPic** is scarce in the literature[21−25] despite its simple structure. By contrast, fluorine that is arguably the most utilized halogen substituent has been used because of its peculiarity to shift emission maxima of the cyclometalated iridium complexes to higher energy. In particular, **FIrPic**[26,27] is one of the commercially available and widely studied neutral cyclometalated iridium complexes and therefore can be taken as a benchmark for comparing properties of other similar iridium complexes. Thus, we prepared in addition the homologous chloro and bromo complexes, **ClIrPic** and **BrIrPic**, that have not yet been reported in the literature. In all cases, the structural modifications along the series may be considered minor since chemically similar units have been introduced in the same position of the main ligand of the complexes. However, we observed significant changes in the photophysical properties along this series, in particular for **BrIrPic**. We used linear-response time-dependent density functional theory (LR-TDDFT) including spin−orbit coupling (SOC), and unrestricted DFT (U-DFT) to obtain information about this effect. Overall, in addition of the expected heavy atom effect, the changes in emission properties are attributed to a deformation of the excited state geometry caused by the large size of the halogen.

EXPERIMENTAL PROCEDURES

Materials and General Considerations. The solvents (puriss. grade) and commercially available starting materials were used as received. NMR spectra were measured with AV-400 spectrometers, and the reported chemical shifts were referenced to tetramethylsilane, $Si(CH_3)_4$. Mass spectra and elemental analysis have been performed by the services of analysis at EPFL. 2-(2,4-difluorophenyl)pyridine,[28] 2,4-dibromoiodobenzene[29] and 2-(allyldimethylsilyl)pyridine[30] have been prepared following the literature. We reported the synthesis of 2-(2,4-chlorophenyl)pyridine and **HIrPic** previously.[25]

Theoretical Calculations. Full geometry optimizations of the iridium compounds in their singlet ground state were performed with DFT using the M06 functional,[31] with the relativistic effective core potential and basis set LANL2DZ[32] for the iridium and the 6-311G*[33] basis set for the remaining atoms. The use of more flexible basis sets including diffuse functions showed no significant changes in the main geometrical features of the optimized compounds. No symmetry constraints were applied during the geometry optimizations, which were carried out with the Gaussian 09 package.[34] The nature of the stationary points located was further checked by computations of harmonic vibrational frequencies at the same level of theory. At each ground state (singlet) geometry, LR-TDDFT calculations were performed using the same basis sets and *xc*-functional. To cover the experimental range, the first 140 vertical excitations (singlet and triplet) were considered. Condensed-phase effects were taken into account using a self-consistent reaction-field (SCRF) model in which the solvent is implicitly represented by a dielectric continuum characterized by its relative static dielectric permittivity ε. The solute, which is placed in a cavity created in the continuum after spending some cavitation energy, polarizes the continuum, which in turn creates an electric field inside the cavity. Within the different approaches that can be followed to calculate the electrostatic potential created by the polarized continuum in the cavity, we have employed the integral equation formalism of the polarizable continuum model (IEFPCM).[35] As the solvent molecules have no time to geometrically rearrange within the time of a vertical excitation, nonequilibrium solvation[36] has been used for the LR-TDDFT calculations of absorption spectra. A relative permittivity of 8.93 (35.69) was employed to simulate dichloromethane (acetonitrile),[34] the solvents used in the experimental work. SOC LR-TDDFT was performed with the ADF2009[37,38] package using the ZORA methodology.[39] All electron basis sets have been used for all the atoms (iridium: TZP, all other atoms: DZP). To gain insights into the phosphorescence behavior of the different iridium compounds, we optimized the geometry of the first triplet state using unrestricted DFT (U-DFT) with the same basis set as described before. As suggested by a recent work,[40] we used the *xc*-functional M05-2X[41] for this task, because of its excellent performance for the emission spectra for a series of iridium-based compounds. At the minimum energy structure, we computed the difference in energy between the triplet (T_1) and singlet (S_0) with the inclusion of implicit solvent and obtained an estimation of the first phosphorescence band. See Supporting Information for additional details on the calculations.

Spectroscopic Measurements. Absorption spectra were recorded with a Perkin-Elmer λ950 spectrophotometer. For luminescence experiments, the samples were placed in fluorimetric 1-cm path cuvettes and, when necessary, purged from oxygen by bubbling with argon. Uncorrected emission spectra were obtained with an Edinburgh FLS920 spectrometer equipped with a peltier-cooled Hamamatsu R928 photomultiplayer tube (185−850 nm). An Edinburgh Xe900 450 W xenon arc lamp was used as exciting light source. Corrected spectra were obtained via a calibration curve supplied with the instrument. Photoluminescence quantum yields (PLQY, Φ_{em}) in solution obtained from spectra on a wavelength scale (nm) were measured according to the approach described by Demas and Crosby[42] using air-equilibrated $[Ru(bpy)_3]Cl_2$ in aqueous solution [Φ_{em} = 0.028][43] as standard. Emission lifetimes in the ns-μs range were determined with the single photon counting technique by means of the same Edinburgh FLS920 spectrometer using a laser diode as excitation source (1 MHz, λ_{exc} = 407 nm, 200 ps time resolution after deconvolution) and the above-mentioned PMT as detector. Or, with an IBH single photon counting spectrometer equipped with a thyratron gated nitrogen lamp working in the range 2−40 kHz (λ_{exc} = 337 nm, 0.5 ns time resolution) or by using pulsed NanoLED excitation sources at 278 nm, 331 nm, 465 nm, and 560 nm (pulse width ≤0.3 ns); the detector was a red-sensitive (185−850 nm) Hamamatsu R-3237-01 photomultiplier tube. Analysis of the luminescence decay profiles versus time was accomplished with the DAS6 Decay Analysis Software provided by the manufacturer. To record the 77 K luminescence spectra, the samples were put in glass tubes (2 mm diameter) and inserted in a special quartz dewar, filled up with liquid nitrogen.

Cyclic Voltammetric Measurements. A PC controlled AutoLab PSTAT10 electrochemical workstation has been employed. Cyclic voltammograms (CV) were obtained at a scan rate of 100 mV/s using 0.1 M $TBAPF_6$ as supporting electrolyte in acetonitrile. Glassy carbon, sputtered platinum, and platinum wire were employed as working, counter, and reference electrodes, respectively. At the end of each measurement, the ferrocinium/ferrocene (Fc^+/Fc) potential was measured and used as an internal reference.

X-ray Crystal Structure Determination. The data collections for the three crystal structures were measured at low temperature using

dx.doi.org/10.1021/ic2011474 | Inorg. Chem. 2012, 51, 799−811

Mo K_α radiation. An Oxford Diffraction Sapphire/KM4 CCD was employed for **BrIrPic** while the remaining samples were measured on a Bruker APEX II CCD. Both diffractometers have a kappa geometry goniometer. Data reduction were carried out by Crysalis PRO[44] (**BrIrPic**), and EvalCCD[45] (**FIrPic, ClIrPic**) and then corrected for absorption.[46] The solutions and refinements were performed by SHELX.[47] The structures were refined using full-matrix least-squares based on F^2 with all non hydrogen atoms anisotropically defined. Hydrogen atoms were placed in calculated positions by means of the "riding" model. Disorder problems dealing with the solvent (CH_2Cl_2) were found during the refinement of **BrIrPic**. In this case some restraints were applied (SHELX cards: ISOR and DFIX) to get reasonable parameters.

2-(2,4-Bromophenyl)pyridine 3. A mixture of 2-(allyldimethylsilyl)pyridine (1.77 g, 10.0 mmol), 2,4-dibromoiodobenzene (4.70 g, 13.0 mmol), Ag_2O (3.47 g, 15.0 mmol), and $Pd(PPh_3)_4$ (635 mg, 0.55 mmol) in dry tetrahydrofuran (THF, 50.0 mL) was stirred at 60 °C for 10 h under Ar. After cooling the reaction mixture to room temperature, the mixture was filtered on a short silica gel pad. The crude mixture was chromatographed on silica gel (hexane/EtOAc = 50/50 as eluent) to afford 2-(2,4-bromophenyl)pyridine (2.08 g, 66%) as white solid. ^{1}H NMR ($CDCl_3$, 400 MHz): δ 8.72 (1H, dt, J = 7.0, 2.0 Hz); 7.86 (1H, d, J = 5.5 Hz); 7.77 (1H, td, J = 7.6, 2.0 Hz); 7.60 (1H, dt, J = 7.2, 1.5 Hz); 7.55 (1H, dd, J = 7.0, 2.2 Hz); 7.43 (1H, d, J = 7.2 Hz); 7.32 (1H, ddd, J = 7.0, 3.5, 1.2 Hz). TOF MS ES: MH^+ m/z: calc. 313.9003 found: 313.8951.

[Ir(2-(2,4-difluorophenyl)pyridine)$_2$Cl]$_2$ 5. A solution of $IrCl_3{\cdot}xH_2O$ (1.07 g, 3.03 mmol) in a mixture 2-ethoxyethanol/water (60 mL/20 mL) was degassed by bubbling argon for 15 min while heating at 80 °C. **1** (1.28 g, 6.70 mmol) was added as a solid, and the mixture heated at 135 °C for 20 h. After cooling down to room temperature, water (150 mL) was added, and the mixture kept in the fridge for 2 h. The precipitate was filtered on fritted (G4) glass, washed with water (6 × 50 mL), MeOH (50 mL), and hexane (3 × 50 mL) and dried under vacuum to afford **5** as a bright yellow solid (1.31 g, yield 71%). ^{1}H NMR ($CDCl_3$, 400 MHz): δ 9.12 (1H, d, J = 6.0 Hz); 8.31 (1H, d, J = 7.6 Hz); 7.83 (1H, t, J = 7.2 Hz); 6.83 (1H, t, J = 6.4 Hz); 6.34 (1H, t, J = 10.4 Hz); 5.28 (1H, dd, J = 7.4, 1.2 Hz). TOF MS ES: [Ir(2-(2,4-difluorophenyl)pyridine)$_2$]$^+$ m/z: calc. 573.0566 found: 573.0672; [Ir(2-(2,4-difluorophenyl)-pyridine)$_2$(MeCN)]$^+$ m/z: calc. 614.0831 found: 614.0510; [Ir(2-(2,4-difluorophenyl)pyridine)$_2$(MeCN)$_2$]$^+$ m/z: calc. 655.1097 found: 655.1145; {[Ir(2-(2,4-difluorophenyl)pyridine)$_2$](μ-Cl)[Ir(2-(2,4-difluorophenyl)pyridine)$_2$(MeCN)]}$^+$ m/z: calc. 1222.1086 found: 1222.0740.

[Ir(2-(2,4-dichlorophenyl)pyridine)$_2$Cl]$_2$ 6. As **5**, using $IrCl_3{\cdot}xH_2O$ (210 mg, 0.60 mmol), and **2** (290 mg, 1.30 mmol). **6** was obtained as a yellow solid (361 mg, yield 90%). ^{1}H NMR ($CDCl_3$, 400 MHz): δ 9.16 (1H, d, J = 5.6 Hz); 9.08 (1H, d, J = 8.0 Hz); 7.87 (1H, t, J = 7.6 Hz); 6.93 (1H, d, J = 2.0 Hz); 6.89 (1H, td, J = 2.8, 1.2 Hz); 5.55 (1H, d, J = 2.0 Hz). TOF MS ES: [Ir(2-(2,4-dichlorophenyl)pyridine)$_2$]$^+$ m/z: calc. 636.9383 found: 636.9857; [Ir(2-(2,4-dichlorophenyl)pyridine)$_2$(MeCN)]$^+$ m/z: calc. 677.9649 found: 677.9795; [Ir(2-(2,4-dichlorophenyl)pyridine)$_2$(MeCN)$_2$]$^+$ m/z: calc. 718.9915 found: 719.0273; {[Ir(2-(2,4-dichlorophenyl)pyridine)$_2$]-(μ-Cl)[Ir(2-(2,4-dichlorophenyl)pyridine)$_2$(MeCN)]}$^+$ m/z: calc. 1349.8722 found: 1349.8344.

[Ir(2-(2,4-dibromophenyl)pyridine)$_2$Cl]$_2$ 7. As **5**, using $IrCl_3{\cdot}xH_2O$ (155 mg, 0.44 mmol), and **3** (303 mg, 0.97 mmol). **7** was obtained as a yellow solid (318 mg, yield 85%). ^{1}H NMR ($CDCl_3$, 400 MHz): δ 9.27 (1H, d, J = 8.4 Hz); 9.13 (1H, dd, J = 6.0, 1.2 Hz); 7.89 (1H, t, J = 7.6 Hz); 7.31 (1H, d, J = 2.0 Hz); 6.91 (1H, td, J = 2.8, 1.2 Hz); 5.70 (1H, d, J = 2.0 Hz). TOF MS ES: [Ir(2-(2,4-dibromophenyl)pyridine)$_2$(MeCN)]$^+$ m/z: calc. 853.7629 found: 853.5371; [Ir(2-(2,4-dibromophenyl)pyridine)$_2$(MeCN)$_2$]$^+$ m/z: calc. 894.7894 found: 894.5612.

FIrPic. Picolinic acid (154 mg, 1.25 mmol, ~3 equiv) and tetrabutyl ammonium hydroxide (1.66 g, 2.1 mmol, ~5 equiv) were added to a solution of **5** (505 mg, 0.42 mmol) in dichloromethane (150 mL). The yellow solution was refluxed under argon overnight. After cooling down to room temperature, the solution was filtered on cellite, and evaporated to dryness to give a yellow viscous oil which precipitated upon addition of methanol (30 mL). The suspension was kept in the fridge for 2 h, filtered off, and washed with cold methanol (30 mL) and hexane (100 mL). The solid was adsorbed on silica, deposited on the top of a silica gel chromatography column, and eluted with dichloromethane. Finally, the main yellow fraction was dissolved in a minimum amount of a methanol/dichloromethane mixture (10/90, v:v) and slowly precipitated with hexane. The suspension was filtered off, washed with hexane and dried to afford **FIrPic** as a bright yellow solid (473 mg, yield 82%). ^{1}H NMR ($CDCl_3$, 400 MHz): δ 8.75 (1H, d, J = 4.8 Hz); 8.34 (1H, d, J = 7.6 Hz); 8.30 (1H, d, J = 4.4 Hz); 8.24 (1H, d, J = 8.4 Hz); 7.95 (1H, dt, J = 7.6, 1.2 Hz); 7.78–7.74 (3H, m); 7.45–7.41 (2H, m); 7.19 (1H, t, J = 6.0 Hz); 6.97 (1H, t, J = 6.0 Hz); 6.50 (1H, t, J = 9.6 Hz); 6.40 (1H, t, J = 9.6 Hz); 5.82 (1H, dd, J = 7.6, 1.6 Hz); 5.57 (1H, dd, J = 8.2, 2.0 Hz). TOF MS ES: MH^+ m/z: calc. 696.0881 found: 696.0895. Anal. Calcd. for $C_{28}H_{16}F_4IrN_3O_2$: C, 48.41; H, 2.32; N, 6.05. Found: C, 48.38; H, 2.48; N, 5.92.

ClIrPic. As **FIrPic** using **6** (130 mg, 0.10 mmol), picolinic acid (36 mg, 0.30 mmol) and tetrabutyl ammonium hydroxide (388 mg, 0.50 mmol). **ClIrPic** was obtained as a yellow solid (127 mg, 87%). ^{1}H NMR ($CDCl_3$, 400 MHz): δ 9.11 (1H, d, J = 6.8 Hz); 9.02 (1H, d, J = 6.8 Hz); 8.81 (1H, d, J = 5.6 Hz); 8.33 (1H, d, J = 7.6 Hz); 7.95 (1H, dt, J = 7.6, 1.2 Hz); 7.85–7.79 (2H, m); 7.72 (1H, d, J = 4.8 Hz); 7.50 (1H, d, J = 5.2 Hz); 7.43 (1H, td, J = 5.2, 1.2 Hz); 7.26 (1H, td, J = 5.2, 1.2 Hz); 7.08 (1H, d, J = 2.0 Hz); 7.02 (1H, td, J = 6.0, 1.2 Hz); 7.02 (1H, d, J = 2.0 Hz); 6.16 (1H, d, J = 2.0 Hz); 5.84 (1H, d, J = 1.6 Hz). ^{13}C NMR ($CDCl_3$, 100 MHz): δ 175.99, 171.93, 165.62, 164.19, 152.35, 151.57, 151.06, 148.47, 147.78, 147.49, 138.41, 138.26, 137.87, 137.24, 134.55, 134.06, 131.07, 130.88, 130.12, 129.92, 128.07, 127.91, 124.69, 124.13, 124.02, 123.56, 122.96, 122.72. TOF MS ES: MH^+ m/z: calc. 759.9683 found: 759.9684 Anal. Calcd. for $C_{28}H_{16}Cl_4IrN_3O_2{\cdot}CH_3OH$: C, 43.95; H, 2.54; N, 5.30. Found: C, 44.18; H, 2.48; N, 4.98.

BrIrPic. As **FIrPic** using **7** (130 mg, 0.076 mmol), picolinic acid (38 mg, 0.31 mmol) and tetrabutyl ammonium hydroxide (470 mg, 0.59 mmol). **BrIrPic** was obtained as a yellow solid (113 mg, 79%). ^{1}H NMR ($CDCl_3$, 400 MHz): δ 9.30 (1H, d, J = 6.8 Hz); 9.22 (1H, d, J = 6.8 Hz); 8.80 (1H, d, J = 5.6 Hz); 8.33 (1H, d, J = 7.6 Hz); 7.95 (1H, dt, J = 7.6, 1.2 Hz); 7.87–7.80 (2H, m); 7.71 (1H, d, J = 4.8 Hz); 7.50 (1H, d, J = 5.2 Hz); 7.49 (1H, d, J = 2.0 Hz); 7.43 (1H, td, J = 5.2, 1.2 Hz); 7.41 (1H, d, J = 2.0 Hz); 7.27 (1H, td, J = 5.2, 1.2 Hz); 7.06 (1H, td, J = 6.0, 1.2 Hz); 6.33 (1H, d, J = 2.0 Hz); 5.99 (1H, d, J = 1.6 Hz). ^{13}C NMR ($CDCl_3$, 100 MHz): not measured because of low solubility. TOF MS ES: MH^+ m/z: calc. 939.7654 found: 939.7634 Anal. Calcd. for $C_{28}H_{16}Br_4IrN_3O_2$: C, 35.84; H, 1.72; N, 4.48. Found: C, 35.77; H, 2.08; N, 4.08.

RESULTS AND DISCUSSION

Synthesis and X-ray Crystal Structures. The ligands **1** and **2** were prepared using Suzuki coupling. The ligand **3** requires a longer synthesis using an allylsilane pyridine intermediate for avoiding mixtures of multisubstituted compounds (Scheme 1). Complexes were prepared in a usual two-step synthesis according to Scheme 2. Reaction of $IrCl_3{\cdot}xH_2O$ with 2.2 equiv of ligand in a mixture 2-ethoxy-ethanol/water at reflux overnight gives the corresponding chloro-bridged iridium(III) dimer in good yield (70–90%) after precipitation, and washing with water, MeOH, and hexane. Subsequent reaction in dichloromethane with 3 equiv of picolinic acid in the presence of 5 equiv of tetrabutyl ammonium hydroxide at reflux overnight gives after workup and purification, the expected **XIrPic** (X = F, Cl, Br) compounds in good yields (80–90%).

Single crystals of **FIrPic**, **ClIrPic**, and **BrIrPic** have been grown by slow diffusion of hexane into a dichloromethane solution of the complexes. Structures are shown in Figure 1 and selected crystallographic data are provided in Table 1 and Table 2.

dx.doi.org/10.1021/ic2011474 | Inorg. Chem. 2012, 51, 799–811

Scheme 1. Synthesis of 2,4-Dibromo-phenyl-pyridine 3 (i) $NaNO_2$, H_2SO_4, KI; (ii) *n*-BuLi, allylchlorodimethylsilane; (iii) $Pd(PPh_3)_4$, Ag_2O

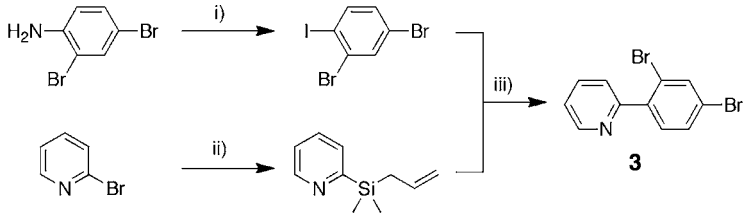

Scheme 2. Chemical Structures of Molecules; (i) 2-ethoxy-ethanol/H_2O, reflux; (ii) CH_2Cl_2, TBAOH, picolinic acid, reflux

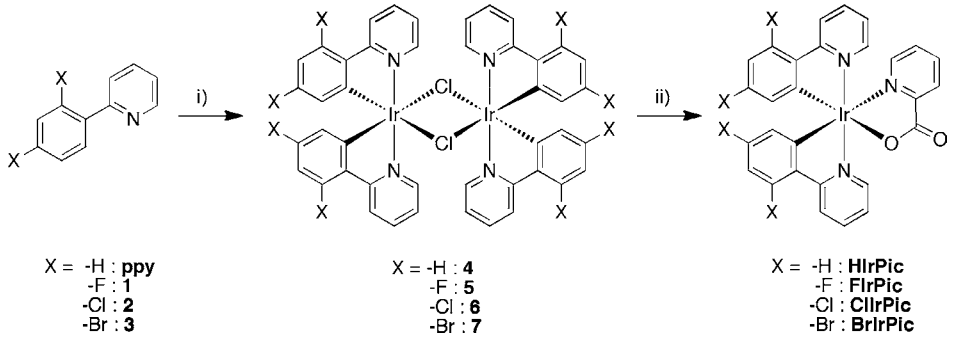

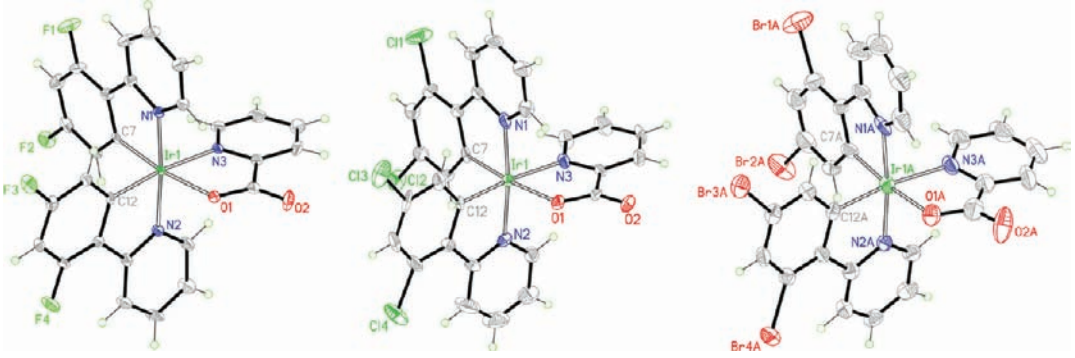

Figure 1. X-ray crystal structure of **FIrPic**, **ClIrPic**, and **BrIrPic**.

Table 1. Comparison between Experimental and Theoretical (DFT/M06) Ground State Geometries[a]

	FIrPic		ClIrPic		BrIrPic[c]	
	X-ray	M06	X-ray	M06	X-ray	M06
			Bond Distance			
Ir–N(1)	2.049(3)	2.05	2.038(6)	2.05	2.039(7)	2.05
Ir–N(2)	2.056(3)	2.06	2.038(6)	2.06	2.041(6)	2.06
Ir–N(3)	2.135(3)	2.19	2.154(6)	2.19	2.137(7)	2.19
Ir–C(7)	2.002(3)	2.00	1.999(7)	2.00	1.989(9)	2.00
Ir–C(12)	2.010(3)	2.01	2.003(7)	2.01	1.996(8)	2.01
Ir–O(1)	2.158(2)	2.18	2.162(5)	2.18	2.139(6)	2.18
C(11)-X(1)[b]	1.369(4)	1.34	1.772(8)	1.76	1.897(10)	1.91
			Bond Angle			
C(7)–Ir–C(12)	88.76(12)	88.6	88.9(3)	89.1	89.7(3)	90.4
C(7)–Ir–N(1)	80.91(11)	80.4	80.1(3)	79.9	79.3(3)	79.9
C(12)–Ir–N(1)	94.63(12)	95.1	95.9(3)	98.7	95.7(3)	95.4
C(7)–Ir–N(3)	96.57(12)	98.2	97.7(3)	96.6	98.8(3)	96.5
C(12)–Ir–O(1)	97.81(11)	97.4	96.8(2)	98.7	94.6(3)	97.3
N(1)–Ir–N(2)	175.17(10)	174.7	174.5(2)	174.8	173.7(3)	174.2

[a]Selected bond distances (Å) and angles (deg). [b]X = F, Cl, or Br. [c]Asymmetric unit contains two independent molecules, the selected values belong to molecule A.

The three complexes have the expected slightly deformed octahedral coordination geometry around the iridium center with the cis-C,C trans-N,N chelate configuration. Overall, there are no large geometric differences among the complexes, the size

dx.doi.org/10.1021/ic2011474 | *Inorg. Chem.* 2012, 51, 799–811

Table 2. Crystallographic Data for FIrPic, ClIrPic, and BrIrPic

	FIrPic·MeOH	**ClIrPic**	BrIrPic·1/2CH_2Cl_2
empirical formula	$C_{29}H_{20}F_4IrN_3O_3$	$C_{28}H_{16}Cl_4IrN_3O_2$	$C_{28.5}H_{17}Br_4ClIrN_3O_2$
formula weight	726.68	760.44	980.74
temperature, K	100(2)	100(2)	140(2)
wavelength (Å)	0.71073	0.71073	0.71073
crystal system	monoclinic	orthorhombic	monoclinic
space group	*C*2/*c*	*Pbca*	*I*2/*a*
unit cell dimensions			
a (Å)	30.723(6)	15.0279(14)	30.6777(6)
b (Å)	10.570(2)	15.440(2)	11.2485(2)
c (Å)	15.488(3)	28.284(3)	35.0954(7)
α (deg)	90	90	90
β (deg)	92.40(3)	90	90.412(2)
γ (deg)	90	90	90
volume (Å^3)	5025.3(17)	6562.6(13)	12110.3(4)
Z	8	8	16
density, calcd (g/cm^3)	1.921	1.539	2.152
absorption coefficient (mm^{-1})	5.382	4.421	9.808
F(000)	2816	2928	7344
crystal size (mm^3)	0.87 × 0.41 × 0.22	0.69 × 0.63 × 0.32	0.35 × 0.31 × 0.22
θ range for data collection (deg)	3.31 to 25.02	3.30−25.03	2.66−25.03
reflections collected	47584	98253	44681
independent reflections	4445 [R(int) = 0.0452]	5710 [R(int) = 0.0577]	10690 [R(int) = 0.0446]
absorption correction	semiempirical from equivalents	semiempirical from equivalents	semiempirical from equivalents
refinement method	full-matrix least-squares on F^2	full-matrix least-squares on F^2	full-matrix least-squares on F^2
data/restraints/parameters	4445/0/361	5710/0/344	10690/39/739
goodness-of-fit on F^2	1.158	1.128	1.077
final *R* indices [$I > 2\sigma(I)$]	R_1 = 0.0185	R_1 = 0.0479	R_1 = 0.0379
	wR_2 = 0.0377	wR_2 = 0.0896	wR_2 = 0.0883
R indices (all data)	R_1 = 0.0259	R_1 = 0.0635	R_1 = 0.0648
	wR_2 = 0.0412	wR_2 = 0.0958	wR_2 = 0.1067

of the halogen atoms having apparently no significant impact. **BrIrPic** shows a more compact octahedral geometry around the central iridium atom than **FIrPic** as bonds involving the iridium are generally shorter with the bromine substituents. **ClIrPic** stands out with a more symmetrical environment around the iridium center since the bonds Ir−N(1) and Ir−N(2) are identical, which is not the case in the other complexes. In addition, the ancillary ligand is less tightly bound as the distances Ir−N(3) and Ir−O(1) are longer than in the other complexes. The only notable consequence of the halogen substituents lies in the carbon−halogen bond lengths and in the distortion of the phenyl-pyridine ligand (see below). The crystal structure of **FIrPic** has been recently reported.[48] The octahedral coordination geometry around the iridium center is slightly more compact than our report, an effect that might be attributed to the absence of cocrystallized solvent. We have reported the X-ray crystal structure of **HIrPic** previously.[25]

Photophysical Properties. The UV−visible electronic absorption spectra of **HIrPic**, **FIrPic**, **ClIrPic**, and **BrIrPic** were recorded in CH_2Cl_2 solution (Figure 2). Though the spectral profiles of the four complexes are quite similar, the onset of absorption of the fluorine-substituted complex shows a significant blue shift compared to the others. The UV region is dominated by intense absorption bands ($\varepsilon \approx 3.8 \times 10^4$ M^{-1} cm^{-1}) assigned to ligand centered (LC) $^1(\pi-\pi^*)$ transitions.[49] The peaks at 256 (**FIrPic**), 262 (**HIrPic**), 264 (**ClIrPic**), and 268 (**BrIrPic**) nm are due to the absorption of cyclometalating ligands F_2ppy, H_2ppy, Cl_2ppy, and Br_2ppy, respectively. The weaker and broader bands at lower energies (350−440 nm, $\varepsilon \approx$ 5000 M^{-1} cm^{-1}) are of charge-transfer (CT) nature and are related to electronic transitions occurring from the metal center to the cyclometalated ligands (MLCT) (see theoretical calculations below).[50]

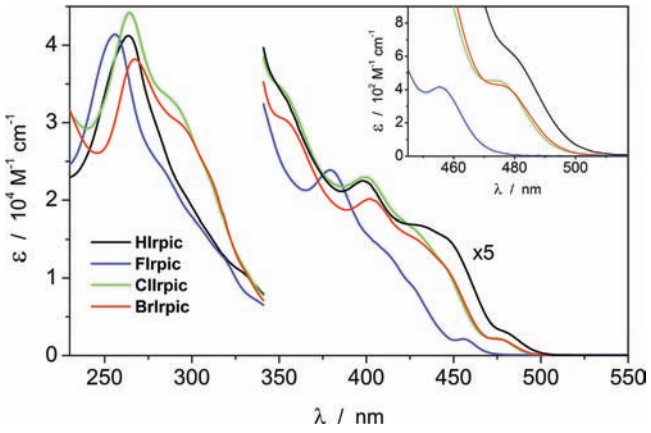

Figure 2. Electronic absorption spectra of **HIrPic** (black), **FIrPic** (blue), **ClIrPic** (green), and **BrIrPic** (red) in dichloromethane solutions at room temperature. The lowest energy T_1 transitions are zoomed in at the top-right inset.

As reported for similar complexes by Thompson et al., this class of compounds exhibits a weak bathochromic shift of MLCT absorption features upon decrease of the solvent polarity (see Supporting Information, Figure S1 to S3), suggesting that the CT state is less polar than the ground state.[51] Moreover,

dx.doi.org/10.1021/ic2011474 | *Inorg. Chem.* 2012, 51, 799−811

the virtually solvent-independent and extremely weak ($\varepsilon \approx 450\ M^{-1}\ cm^{-1}$) absorption bands detected at 455 (**FIrPic**), 474 (**ClIrPic**), 475 (**BrIrPic**), and 480 (**HIrPic**) nm can be attributed to the direct population of the emitting triplet state (T_1). Our theoretical calculations reproduce correctly these low intensity absorption tails by calculating the direct singlet−triplet transitions taking into account the SOC effects (see below). The small spectral shift between the T_1 absorption and emission profiles (<0.1 eV, for all the complexes) at room temperature suggests that the emitting state has some $*\pi-\pi$ character (see below).

The luminescence spectra of the complexes in CH_2Cl_2 are depicted in Figure 3. As for the absorption, the emission profiles

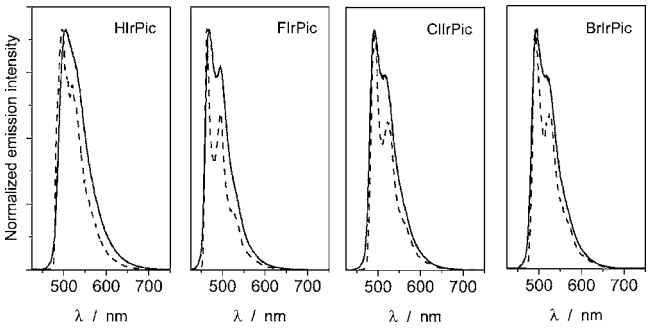

Figure 3. Normalized emission spectra (λ_{exc}= 407 nm) of **HIrPic**, **FIrPic**, **ClIrPic**, and **BrIrPic** in CH_2Cl_2, at room temperature (solid line) and 77 K rigid matrix (dashed line).

of **ClIrPic** (λ_{max} = 491 nm) and **BrIrPic** (λ_{max} = 494 nm) are red-shifted with respect to **FIrPic** (λ_{max} = 468 nm) while **HIrPic** (λ_{max} = 505 nm) is the most red-shifted one. Our theoretical calculations (see below) and previous studies indicate that the picolinate triplet levels lie at rather high energy and are not involved in the electronic transition causing luminescence.[49] For this reason, the picolinate moiety is essentially an ancillary ligand and the luminescence properties are mainly of ^{3}(MLCT−LC) nature, involving iridium d orbitals and $\pi-\pi^*$ orbitals of the halogen-substituted phenylpyridine (*ppy*) cyclometalated units. On the other hand, the LUMO of **HIrPic** has been found to be mainly located on the picolinate ligand.[24] Therefore the use of halogen substituents on the phenyl ring of the main ligand induces a change of the localization of the LUMO of the complexes by stabilizing the LUMO energy levels located on the main cyclometalated ligand (Figure 4, 5, and 6).

The luminescence properties of **FIrPic**, **ClIrPic**, **BrIrPic**, and **HIrPic** are unaffected by changes in the excitation wavelength, and the spectral position of the emission band is not depending on the solvent polarity (Supporting Information, Figure S1 to S3). This last feature and the well-resolved vibronic progressions displayed by all the emission profiles indicate that, in all the cases, the emitting state (T_1) has a predominant ^{3}LC character. In addition, at 77 K (Figure 3), all the samples show very intense and highly resolved bands that exhibit small rigidochromism; a hypsochromic shift of less than 5 nm is observed for **FIrPic** and **BrIrPic** while in the case of **ClIrPic** no shift is detected. The strong similarity between room temperature (RT) and 77 K emission bands, as well as the comparable excited state lifetimes, confirm the weak MLCT character of T_1 at room temperature.[54,55] Finally, the triplet nature of the emitting states

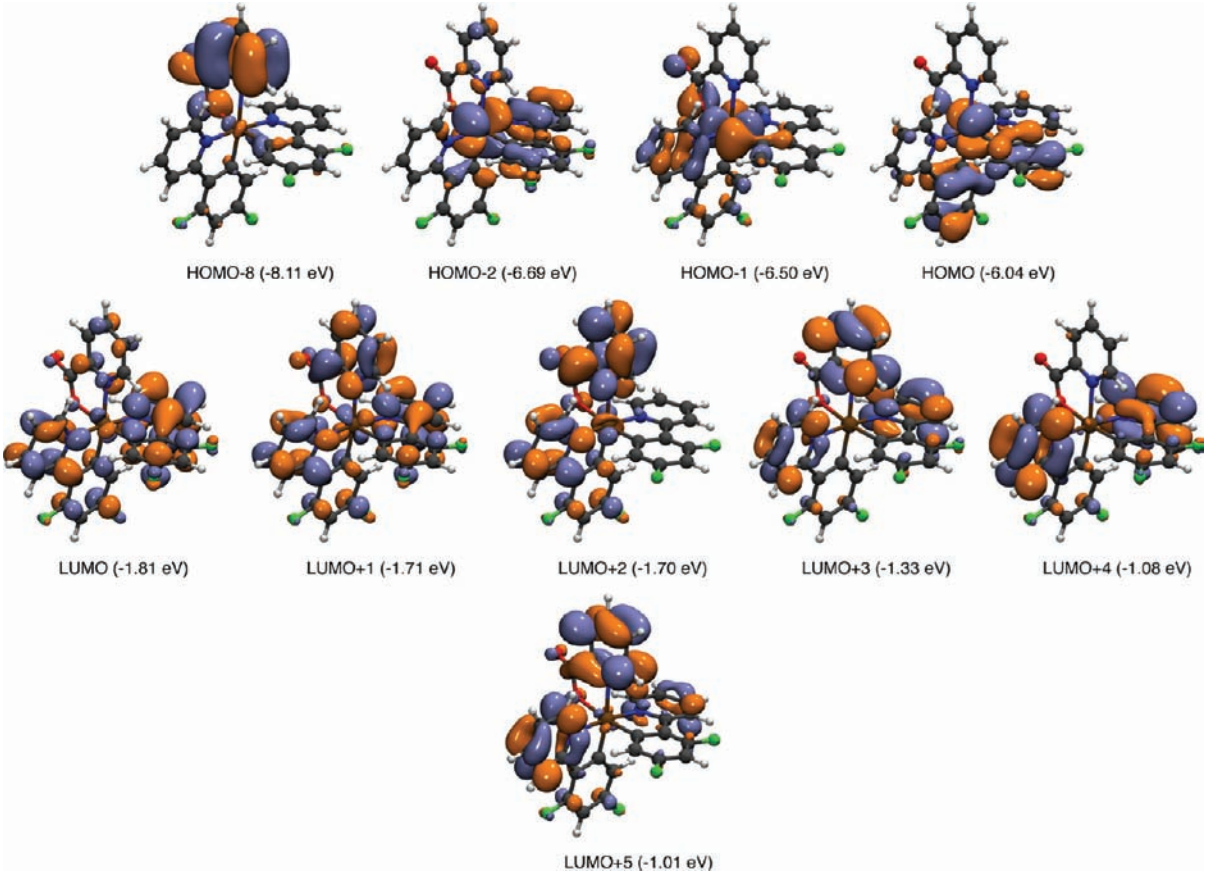

Figure 4. Selected Kohn−Sham molecular orbitals for the characterization of LR-TDDFT excited states of **FIrPic**. Isovalue is set to 0.03 au.

dx.doi.org/10.1021/ic2011474 | *Inorg. Chem.* 2012, 51, 799−811

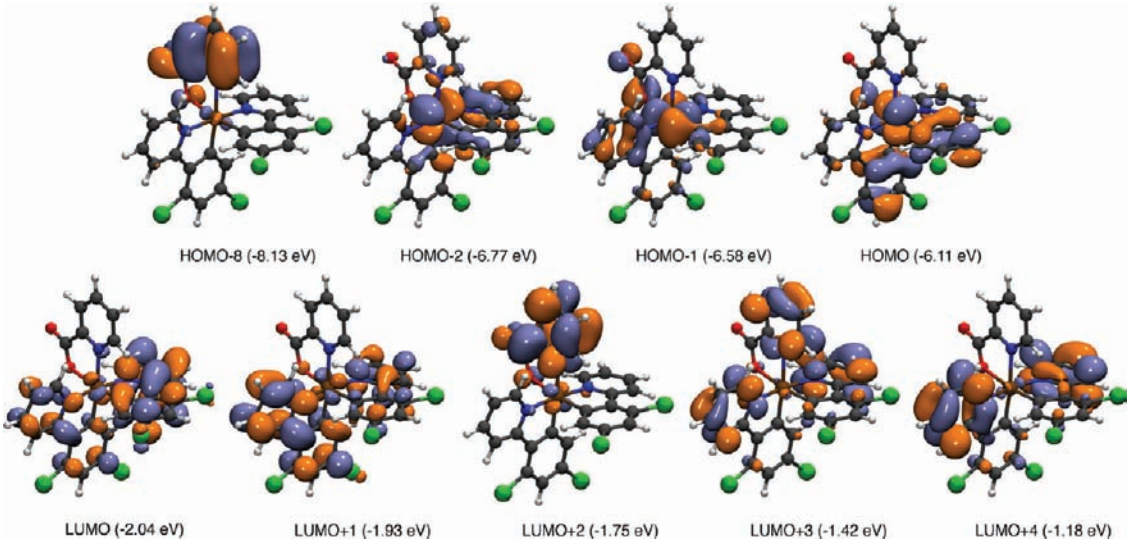

Figure 5. Selected Kohn–Sham molecular orbitals for the characterization of LR-TDDFT excited states of **ClIrPic**. Isovalue is set to 0.03 au.

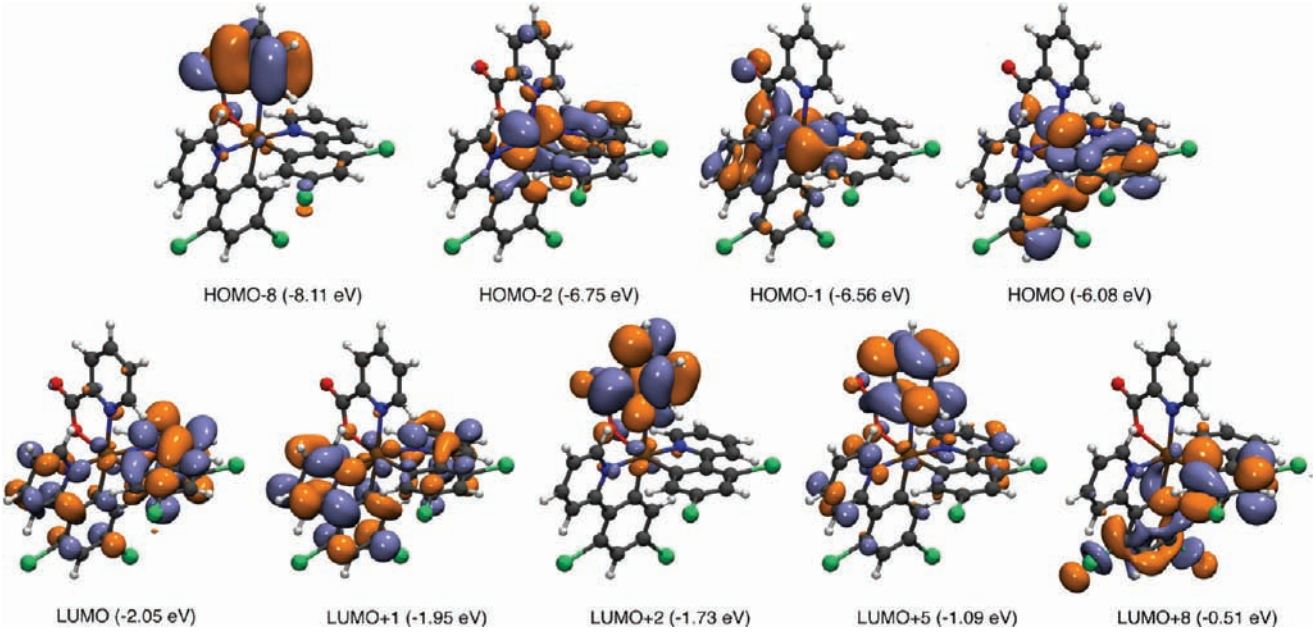

Figure 6. Selected Kohn–Sham molecular orbitals for the characterization of LR-TDDFT excited states of **BrIrPic**. Isovalue is set to 0.03 au.

Table 3. Photophysical Data of the Investigated Complexes at Room and Low Temperature

	298 K emission[a]				deactivation rate constants[c,d]		77 K emission[c]	
sample	λ_{max} [nm]	Φ_{em} [%][b]	τ [ns]		k_r [10^5 s^{-1}]	k_{nr} [10^5 s^{-1}]	λ_{max} [nm]	τ [μs]
HIrPic	505	14.7 (2.2)	514	(74)	2.86	19.17	496, 519	2.98
FIrPic	468, 495	62.0 (3.9)	1722	(103)	3.60	2.20	463, 495	2.24
ClIrPic	491, 517	65.9 (5.1)	2408	(185)	2.73	1.42	491, 522	3.10
BrIrPic	494, 519	9.1 (4.0)	*e*	(145)	biexp.	biexp.	490, 524	2.92

[a]Oxygen-free CH_2Cl_2 solutions, from spectra corrected for the detector response; in brackets, air-equilibrated solutions. [b]Although we are aware that the reference value used for luminescence quantum yield of $[Ru(bpy)_3]_2^+$ in aerated water has been recently re-evaluated and found to be 0.04 (see refs 52 and 53), we prefer to use the value reported for the air equilibrated $[Ru(bpy)_3]Cl_2$ in aqueous solution [Φ_{em} = 0.028] (see ref 43) as the standard, which was also reproduced in house. [c]λ_{exc} = 407 nm. [d]Radiative constant: $k_r = \Phi_{em}\cdot\tau^{-1}$; nonradiative constant: $k_{nr} = \tau^{-1} - k_r$ (assuming unitary intersystem crossing efficiency). [e]t_1 = 1100 (7%), t_2 = 330 (93%).

(highly oxygen sensitive) leads to a strong decrease of PLQY and lifetimes in air-equilibrated solution, as reported in Table 3.

To further support the LC character of the emission, we measured the photophysical properties of the ligands 2-(2,4-di-X-phenyl)pyridine (X = H, F, Cl, Br), **H_2ppy**, **F_2ppy**, **Cl_2ppy**, and **Br_2ppy** (Supporting Information, Figure S4, S5 and S6). As reported in the literature,[56,57] 2-phenylpyridine is not emitting in common organic solvents and only the protonated

dx.doi.org/10.1021/ic2011474 | *Inorg. Chem.* 2012, 51, 799–811

Table 4. Electrochemical Properties of Complexes HIrPic, FIrPic, ClIrPic, and BrIrPic

	E_{ox} /V[a]	E_{HOMO} /eV[b]	$E_{opt\text{-}LUMO}$ /eV[c]	σm	σp	computed −IE/eV[d]	computed EA/eV[e]	computed $E_{opt\text{-}LUMO}$ /eV[f]
HIrPic	0.58	−5.38	−2.92	0	0	−5.46	−2.01	−2.54
FIrPic	0.92	−5.72	−3.07	0.34	0.06	−5.81	−2.10	−2.68
ClIrPic	0.94	−5.74	−3.22	0.37	0.23	−5.85	−2.34	−2.85
BrIrPic	0.95	−5.75	−3.24	0.39	0.23	−5.82	−2.35	−2.84

[a]0.1 M $TBAPF_6$ in acetonitrile, potential vs ferrocene. [b]$E_{HOMO} = -(E_{ox} + 4.8)$. [c]$E_{opt\text{-}LUMO} = E_{HOMO} + E_{0-0}$. [d]Ionization energy DFT/M06. [e]Electron affinity DFT/M06. [f]Computed $E_{opt\text{-}LUMO} = -IE + \Delta E_{LR\text{-}TDDFT}(S_1-S_0)$.

2-phenylpyridinium ion shows significant emission, both in fluorescence and phosphorescence. This is due to a shift in the nature of the transition from $^1n-\pi^*$ to $^1\pi-\pi^*$ upon protonation. Therefore the measurements have been performed in 0.1 N H_2SO_4. In fluorescence, all the protonated ligands display an unstructured emission band around 370 nm. While $\mathbf{H_2ppyH^+}$ and $\mathbf{F_2ppyH^+}$ are characterized by high fluorescent quantum yields (50.0% and 36.0% respectively), it drops considerably for $\mathbf{Cl_2ppyH^+}$ (5.2%) and $\mathbf{Br_2ppyH^+}$ (0.3%). Although a quantitative evaluation of the phosphorescence quantum yield in frozen matrixes is not straightforward, qualitatively the intensity of the phosphorescence emission significantly increases along the series H < F < Cl < Br concomitantly with the drop in fluorescence. This points to an enhanced intersystem crossing because of the increasing heavy atom effect along the halogen series. With heavier halogen substituents, the deactivation of the first singlet-excited state through the triplet is faster. The phosphorescence emission of $\mathbf{F_2ppyH^+}$ (λ_{max} = 445 nm) is 14 nm blue-shifted compared to $\mathbf{H_2ppyH^+}$ (λ_{max} = 459 nm), while the triplet-excited states of $\mathbf{Cl_2ppyH^+}$ and $\mathbf{Br_2ppyH^+}$ are very close in energy (λ_{max} = 453 and 455 nm, respectively). The energy trend follows the one observed for the emission of the **XIrPic** series. In addition the spectral profiles of the ligand triplet emission reflect the structured emission of the corresponding complexes. This evidence confirms that the T_1 emitting state of the **XIrPic** complexes arises from a triplet state with a strong ^{3}LC character, involving mainly the X_2ppy ligands.

ClIrPic and **FIrPic** show remarkable photophysical properties compared to **HIrPic**, that is, high emission intensities (PLQY > 0.6) and long lifetimes (τ > 1.5 μs). On the other hand, the PL performance of **BrIrPic** is poorer (PLQY < 0.1). Assuming unitary intersystem crossing quantum yield, it is possible to calculate radiative (k_r) and nonradiative (k_{nr}) decay rates from phosphorescence quantum yields and lifetimes. This leads to a radiative lifetime τ_{rad} (respectively k_r) of 3.49 μs (2.86×10^5 s^{-1}) for **HIrPic**, 2.77 μs (3.6×10^5 s^{-1}) for **FIrPic**, 3.65 μs (2.73×10^5 s^{-1}) for **ClIrPic**, and 3.62 μs (2.76×10^5 s^{-1}) for **BrIrPic** (using the major component of the biexponential). The radiative constants are similar for all complexes and cannot explain the poor performance of **BrIrPic**. Therefore nonradiative processes are significantly more active in **BrIrPic** than in the other complexes. In addition of the heavy atom effect, they appear to be favored by the significant geometrical distortion of the excited state induced by the large bromine atom (see below).

Electrochemistry. The oxidation potentials of the prototype complex **HIrPic** and of the three halogenated compounds have been measured by cyclic voltammetry in acetonitrile solution containing 0.1 M tetrabutyl ammonium hexafluorophosphate ($TBAPF_6$). The complexes show reversible processes at 0.58, 0.92, 0.94, and 0.95 V vs ferrocene for the nonhalogenated, the fluoro, the chloro, and the bromo complexes, respectively, because of the oxidation of the iridium center. This shows that the HOMOs are stabilized as expected because of the replacement of H with the stronger acceptor fluoro, chloro, and bromo substituents (Table 4). While the reduction of **FIrPic** is quasi-reversible (−2.29 vs $Fc^{+/0}$), it is not the case for **ClIrPic** and **BrIrPic**, where the reductions are irreversible. This makes the direct comparison of the LUMOs energies based on electrochemical measurements poorly reliable. Therefore we calculated the *optical* LUMOs energy, that is, the energy of the LUMOs based on the optical gap as obtained experimentally from the emission spectra of the complexes. In our study focusing on the photophysical properties of the complexes the *optical* LUMO energy is anyway more relevant than the *redox* LUMO. Generally the *optical* LUMO is lower than the *redox* LUMO as the optical gap is smaller than the redox gap mainly because of the exciton binding energy. Several other factors should be taken into account to compare precisely the optical and redox gaps,[58] hence to compare the *optical* LUMO energy with the *redox* LUMO energy. Nevertheless, as a first approximation supported by calculations, it can be assumed that the difference between the optical and redox gaps is constant for closely related molecules.[58] Using this simplification, the trend observed in the calculated *optical* LUMO energies is assumed to be reasonably valid for the *redox* LUMO energies. Computed vertical ionization energies (energy of the oxidized molecule minus the energy of the neutral molecule) and vertical electron affinities (energy of the reduced molecule minus the energy of the neutral molecule) can be taken as an estimator of the experimentally determined $-E_{HOMO}$ and E_{LUMO}, respectively. Both quantities follow closely the experimental trend along the halogen series, with almost constant −IE values for **FIrPic**, **ClIrPic**, and **BIrPic**. Even though the absolute EA values are shifted with respect to $E_{opt\text{-}LUMO}$, the trend between the different compounds is well reproduced with a first energy stabilization step between **HIrPic** and **FIrPic**, and a second one between **FIrPic** and **ClIrPic**/**BrIrPic**. A way to approximate $E_{opt\text{-}LUMO}$ consists in calculating the difference between the computed transition energy of the first singlet state and the ionization energy (see Table 4). This procedure is in fact more closely related to how the experimental $E_{opt\text{-}LUMO}$ is obtained, as we add to the computed E_{ox} (= −IE) the optical gap obtained from LR-TDDFT. These theoretical $E_{opt\text{-}LUMO}$ provide a further good agreement with the observed experimental trend. As the trends for experimental energies of *redox* LUMO and *optical* LUMO are expected to be similar and as the trends for computed EA and $E_{optLUMO}$ are similar, in the discussion about trends hereafter we will use LUMO without distinction.

On the basis of these experimental HOMOs and LUMOs energy levels, we discuss next the observed red shift of the emission maximum for **ClIrPic** and **BrIrPic** compared to **FIrPic**. Besides varying the skeleton of the cyclometalated ligand, strategies for emission color tuning by modifying the HOMO−LUMO gap with substituents are based on simple rules. Indeed the theory (see theoretical part below) tells that

dx.doi.org/10.1021/ic2011474 | Inorg. Chem. 2012, 51, 799−811

Table 5. (Top) DFT/M06 Optimized Geometries of FIrPic, ClIrPic, and BrIrPic,[a] and (Bottom) Most Distorted ppy Ligand Observed in the X-ray Structures in Comparison with the Geometries for the Ground State (S_0) and the First Excited Triplet State (T_1)

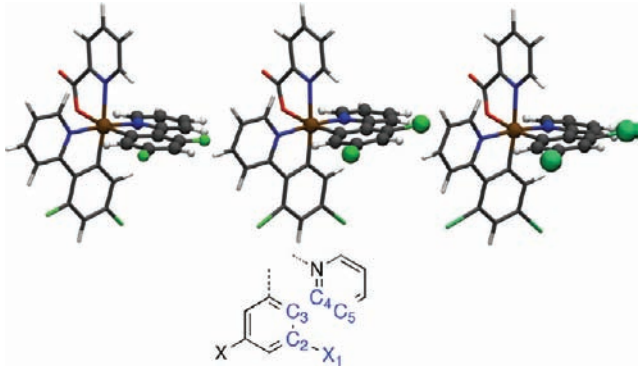

	FIrPic			ClIrPic			BrIrPic			HIrPic		
dihedral angle	X-ray	S_0 M06	T_1 M05-2X	X-ray	S_0 M06	T_1 M05-2X	X-ray	S_0 M06	T_1 M05-2X	X-ray	S_0 M06	T_1 M05-2X
$\delta_1(X_1-C_2-C_3-C_4)$	−0.1	1.2	0.2	2.4	4.3	21.9	6.2	7.2	25.7	1.6	0.4	−1.5
$\delta_2(C_2-C_3-C_4-C_5)$	4.0	3.2	1.7	9.1	11.0	12.1	9.4	14.5	13.5	3.8	4.8	0.6

[a]Distortions on a specific X_2ppy ligand are highlighted by the use of a Ball and Stick representation.

HOMO−LUMO is important in this context for absorption and emission. First, a substituent with donor (acceptor) character will destabilize (stabilize) the energy of the molecular orbital (HOMO and LUMO). Second, the HOMO being mostly localized on the anionic phenyl ring and the LUMO being mostly localized on the neutral part of the cyclometalated ligand (see theoretical part below),[59] that is the pyridine in the present case, a substituent on the anionic part of the ligand will influence the HOMO more than the LUMO; and a substituent on the neutral part of the ligand will influence the LUMO more than the HOMO. In this respect, fluorine substituents on the phenyl ring of a cyclometalated ligand are used to induce a large blue shift of the emission maximum by stabilizing the HOMO much more than the LUMO, overall leading to an increased HOMO−LUMO gap. It should be noted that, experimentally, the position of the substituent is generally critical for the tuning of the HOMO and LUMO energy levels.

As observed from electrochemical data, the slightly stronger acceptor effect of chlorine and bromine compared to fluorine leads to a further stabilization of the HOMO, which translates into a higher oxidation potential. Therefore, the observed red shifts for **ClIrPic** (23 nm) and for **BrIrPic** (26 nm) with respect to **FIrPic** (λ_{em} = 468 nm) indicate that the LUMO levels of the chloride and the bromine derivatives are significantly lower than the LUMO of the fluoro compound. This conclusion is further supported by the theoretical calculations (see below). This effect can be simply rationalized by using the Hammett parameters σm and σp ($\approx \sigma$o), denoting the electronic character of the substituent toward the meta and para ($\approx$ ortho) position respectively.[7] The Hammett parameters have been limited to correlation with oxidation potentials of cyclometalated iridium complexes.[12,60,61] Along the halogens series studied here, σm correlates well with the energy of the HOMO as obtained from electrochemical measurements, and therefore cannot explain the observed red-shift of the emission. On the other hand, the σp values show that the chlorine and the bromine have a much stronger acceptor character than fluorine toward the para ($\approx$ ortho) position. The pyridine, where the LUMO of the complex is mostly localized (see theoretical part below), is in this particular position relative to the halogen substituents. The impact of the chlorine and bromine substituents on the energy of the LUMO will be much stronger than in the case of the fluorine which has a σp value about 1/4 of that of the chlorine and the bromine. This stronger stabilization of the LUMO by chlorine and bromine compared to fluorine, while having similar HOMO energy level, qualitatively explains the observed red shift of emission maxima of **ClIrPic** and **BrIrPic** compared to **FIrPic**. Furthermore correlations of Hammett parameters with computed −IE and computed $E_{optLUMO}$ (Supporting Information, Figure S7) allow a first step toward a quantitative structure−property relationship based solely on Hammett parameters for predicting the emission maxima of cyclometalated iridium complexes with good accuracy (Supporting Information, Figure S8).

DFT Calculations. To gain insight into the electronic structures and the optical properties of the halogen-based complexes we performed DFT/TDDFT calculations on both the ground and the excited states. Structures of **HIrPic**, **FIrPic**, **ClIrPic**, and **BrIrPic** have been optimized in their electronic (singlet) ground state using the exchange and correlation (*xc*) functional M06 (see computational details). The geometrical predictions are in good agreement with the experimental X-ray structures (Table 1) as the root-mean-square deviation (rmsd) between the theoretical and the X-ray coordinates for iridium and the 6 metal-coordinated atoms indicates rather small deviations: 0.04 Å for **FIrPic** and **ClIrPic**, and 0.05 Å for **BrIrPic**. The theoretical geometries present distortions of the ppy ligands, which are due to the steric hindrance induced by the presence of different halogen substituents. The distortion along the halogen series follows the trend observed in the X-ray structures (the most distorted ppy ligands are reported in Table 5) and can significantly impact the optical properties of the compounds, as observed in a previous work (see below for a more extended discussion).[62]

The analysis of excitation energies of the different iridium complexes requires a characterization of the molecular orbitals involved in the different transitions. For all three complexes, the HOMO Kohn−Sham (KS) molecular orbital has an important 5d contribution of 56% in **FIrPic** and of 41% in **ClIrPic** and **BrIrPic** (Table 6). The remaining contributions come from π

dx.doi.org/10.1021/ic2011474 | Inorg. Chem. 2012, 51, 799−811

Table 6. Main Vertical Excitations of FIrPic, ClIrPic, BrIrPic, Computed at the Singlet Electronic Ground State Minimum Energy Structure (LR-TDDFT/M06)[a]

	singlet state	E (nm)	oscillator strength	dominant character
FIrPic				
1	S_1	396.5	0.0491	H→L (85.8%)
2	S_5	338.7	0.0597	H-1→L+1 (67.2%)
3	S_{15}	294.0	0.1177	H-1→L+3 (32.0%)
4	S_{19}	280.8	0.1045	H-1→L+4 (64.2%)
5	S_{30}	264.3	0.1745	H-2→L+5 (43.8%)
6	S_{49}	234.1	0.1317	H-8→L+2 (23.6%)
ClIrPic				
1	S_1	413.6	0.0595	H→L (93.6%)
2	S_5	348.5	0.1005	H-1→L+1 (77.0%)
3	S_{15}	298.3	0.1302	H-1→L+3 (57.2%)
4	S_{22}	280.7	0.1993	H-1→L+4 (32.4%)
5	S_{53}	235.3	0.0486	H-8→L+2 (25.6%)
BrIrPic				
1	S_1	416.2	0.0668	H→L (93.8%)
2	S_5	353.2	0.1128	H-1→L+1 (69.4%)
3	S_{12}	309.8	0.1783	H-2→L+2 (59.6%)
4	S_{14}	304.8	0.1774	H→L+5 (40.0%)
5	S_{29}	269.7	0.3646	H→L+8 (72.6%)
6	S_{62}	234.3	0.0661	H-8→L+2 (15.6%)

[a]The excited singlet state is labeled "S_n", where "n" is the electronic state number according to LR-TDDFT/M06. Only the dominant orbital character is reported.

orbitals located on ppy ligands. In a similar way, the HOMO-1 and HOMO-2 KS orbitals of all studied complexes are combinations of 5d(Ir) and π(ppy) orbitals. All LUMOs can be described as π*-ligand centered orbitals. It is interesting to note that the LUMO of **FIrPic** is more delocalized over the two ppy moieties than in **ClIrPic** and **BrIrPic**, and also presents a contribution from the pic ligand (Figure 4, 5, and 6). LUMO+1 is symmetrically equivalent to the LUMO with respect to the ppy ligand in both **ClIrPic** and **BrIrPic**. Within the energetically lower lying unoccupied KS orbitals we also find contributions from MOs at the pic ligand. This is the case in all studied complexes and is particularly strong in **FIrPic**. Finally, contributions from the σ*(C-X) ppy-based orbitals of **ClIrPic** and **BrIrPic** appear already at LUMO+8 (see for example Figure 6).

LR-TDDFT[63,64] has been used to study the absorption spectra of **FIrPic**, **ClIrPic**, and **BrIrPic**. The first vertical singlet and triplet excitations have been computed to reproduce the full experimental spectra and validate the methodology. The main contributions of the different theoretical peaks with significant oscillator strength are listed in Table 6. The LR-TDDFT excitations are analyzed in terms of electronic transitions between occupied and unoccupied KS orbitals, and only the dominant character of each excited state is listed in the same table. However, in the most general case, several KS molecular orbital transitions characterize a simple LR-TDDFT excitation. In Figures 7, 8, and 9, LR-TDDFT excitation energies are compared with the experimental spectra. To facilitate the comparison, a broadening of the transitions with Gaussians of width 0.37 eV is applied to all spectra.

The agreement between theory and experiment is generally good. Even if the calculated oscillator strengths do not always match perfectly the experimental absorption, the positions of the different bands and their shoulders are rather well described

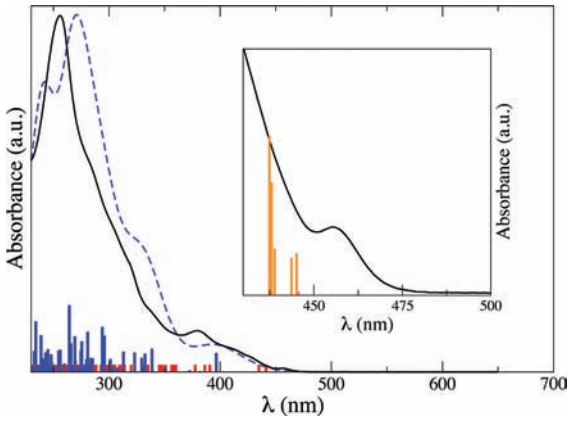

Figure 7. Absorption spectrum of **FIrPic**. Experimental spectrum (black lines) is superimposed on LR-TDDFT/M06 convoluted absorption spectrum (dashed blue line). Singlet (triplet) vertical excitations energies are represented by blue (red) bars. Inset: zoom on the low energy tail of the absorption spectrum, on which ZORA/LR-TDDDT first vertical transitions are superimposed.

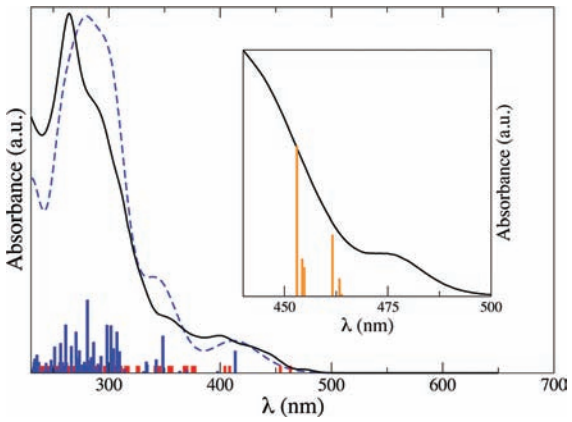

Figure 8. Absorption spectrum of **ClIrPic**. Experimental spectrum (black lines) is superimposed on LR-TDDFT/M06 convoluted absorption spectrum (dashed blue line). Singlet (triplet) vertical excitations energies are represented by blue (red) bars. Inset: zoom on the low energy tail of the absorption spectrum, on which ZORA/LR-TDDDT first vertical transitions are superimposed.

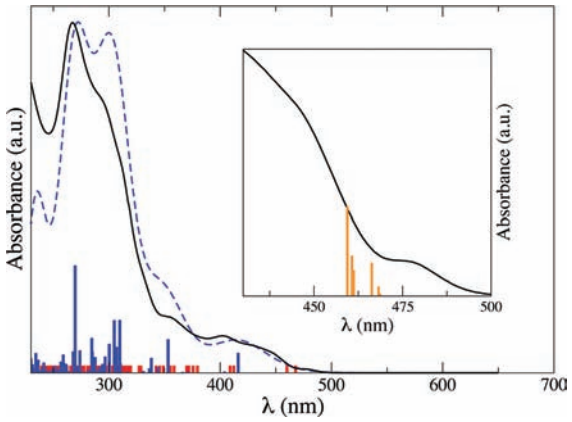

Figure 9. Absorption spectrum of **BrIrPic**. Experimental spectrum (black lines) is superimposed on LR-TDDFT/M06 convoluted absorption spectrum (dashed blue line). Singlet (triplet) vertical excitations energies are represented by blue (red) bars. Inset: zoom on the low energy tail of the absorption spectrum, on which ZORA/LR-TDDDT first vertical transitions are superimposed.

dx.doi.org/10.1021/ic2011474 | *Inorg. Chem.* 2012, 51, 799–811

by the M06 functional. The first experimental bands (350 to 440 nm) were assigned to MLCT transitions, which is in good agreement with the theoretical predictions (Table 6). The three compounds present indeed a common first transition (toward S_1) of HOMO→LUMO type, where the HOMO is mainly a 5d(Ir) orbital and the LUMO is mainly a π^* orbital localized on one ppy ligand (**FIrPic**: 396.5 nm, **ClIrPic**: 413.6 nm, **BrIrPic**: 416.2 nm). The second computed band is attributed to a transition to the fifth singlet excited state (S_5), which involves another 5d(Ir)-based orbital (HOMO-1) and a π^* orbital mainly localized on the second ppy ligand (LUMO+1). We may assign this transition to the experimentally observed shoulder at 340 nm (**FIrPic**), 352 nm (**ClIrPic**), and 354 nm (**BrIrPic**). Note that the measured red shift along the halogen series is also reproduced by the calculations. Other transitions with MLCT character are obtained at higher energies in all three compounds. These states have often an important contribution from the pic ligand, and in the case of **ClIrPic** and **BrIrPic** they are responsible for the shoulder at around 300 nm. As observed experimentally, $^1(\pi-\pi^*)$ transitions become more important in the UV region of the spectra. Of interest is, for example, the $\pi-\pi^*$ contribution of the pic ligand to the band around 235 nm. The first transitions to singlet states of metal-centered (MC) character are observed at rather high energies: above 275 nm for **FIrPic**, 281 nm for **ClIrPic**, and 292 nm for **BrIrPic**.

Concerning singlet-to-triplet transitions, the first transitions occur at 442 and 435 nm (**FIrPic**), 463 and 454 nm (**ClIrPic**), 468 and 460 nm (**BrIrPic**). These are mainly composed by HOMO→LUMO and HOMO→LUMO+1 transitions, respectively, and can thus be considered to be of MLCT type. Previous studies[65,66] have proposed that because of the strong SOC of iridium complexes these singlet-to-triplet transitions could contribute to the low energy tail of the absorption spectra. To validate this proposition in the case of our three compounds, we have performed a series of additional calculations including the effect of SOC using the ZORA approach (see computational details). The results are presented in the inset of Figures 7, 8, and 9, which shows the first six transitions with their corresponding oscillator strengths. Because of the size of SOC, these transitions become slightly allowed and contribute indeed to the experimentally observed absorption tail at low energy, even though an overall blue shift of these weak absorptions is observed in the calculation. As in the case of the corresponding singlet-to-triplet transitions, the character of these spin−orbit allowed excitations is mainly of MLCT type.

To gain some information about the emission processes in **FIrPic**, **ClIrPic**, and **BrIrPic**, we performed, starting from the ground state singlet geometry, unrestricted DFT (U-DFT) geometry optimizations of the first triplet state (T_1) using the *xc*-functional M05-2X. This functional has indeed provided singlet-to-triplet DFT energies in very good agreement with experimental emission spectra for a series of iridium complexes.[40] At the optimized T_1 geometries, we computed both lowest-energy triplet and singlet state energies using an implicit solvent model. The difference of these energies gives an estimate of the position of the first phosphorescence peak. It is important to note here that these Δ-SCF calculations do not take the overlap between the excited and ground state vibrational states into account, which would be needed for the calculation of the Franck−Condon factor. Nonetheless the theoretical values obtained are in rather good agreement with the experimental emission spectra. **FIrPic** shows a theoretical band at 2.66 eV (exp: 2.65 eV), **ClIrPic** at 2.44 eV (exp: 2.52 eV), and **BrIrPic** at 2.40 eV (exp: 2.51 eV). The experimentally observed red shift along the series of compounds is also captured by the calculations while the average discrepancy in the peak positions with respect to the experimental values lies within the accuracy of the method. The same singlet-to-triplet energy gap can also be computed with a LR-TDDFT calculation with spin-flip. In this case, we obtain excitation energies of 2.36 eV for **FIrPic**, 2.18 eV for **ClIrPic**, and 2.15 eV for **BrIrPic**. Even though the LR-TDDFT values are clearly downshifted, the energy differences between the **FIrPic** transition and the ones of the two other compounds are in good agreement with the Δ-SCF calculation. For this transition, LR-TDDFT shows for all three compounds a dominant (>70%) HOMO→LUMO character with a tiny (15−20%) HOMO→LUMO+1 contribution. In agreement with the Δ-SCF DFT calculations, LR-TDDFT/M05-2X predicts therefore a transition to an orbital mainly localized on a single ppy ligand. This result is also confirmed by the analysis of the spin density obtained with the Δ-SCF approach and, equivalently, by the transition density difference computed with LR-TDDFT (Figure 10). These findings are in good agreement with the

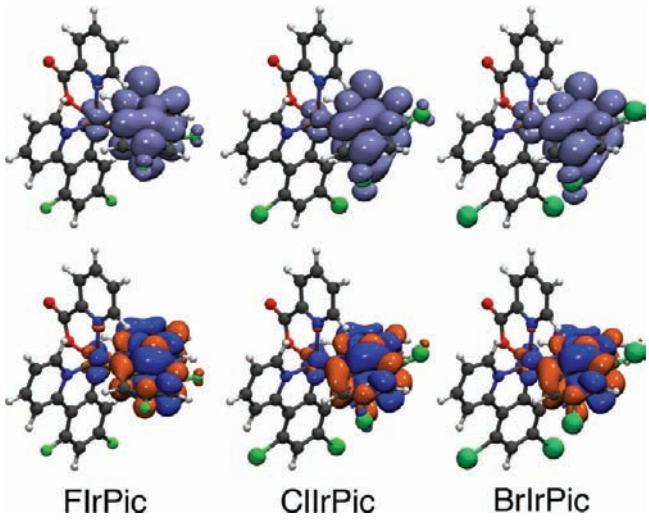

Figure 10. Spin density (upper part) resulting from the unrestricted DFT calculations of the first triplet state. Density differences (lower part) between the first LR-TDDFT triplet state electronic density and the ground state electronic density (positive part in red, negative one in blue). Isovalue is set to 0.002 (0.001) for the spin density (density difference).

experimental observations, where the presence of vibronic structures on the emission spectra suggests an important LC character associated with this transition.

As discussed above, the ground state geometries of **FIrPic**, **ClIrPic**, and **BrIrPic** exhibit already some distortion compared to the optimized nonhalogenated **HIrPic** ground state structure. This distortion is very small in **FIrPic** and becomes more important as the size of halogen atom increases (Table 5). At the optimized T_1 geometry, there is a strong increase of the distortion angle δ_1 in the case of **ClIrPic** and **BrIrPic**. In addition, the deformation is now specifically located on the ppy ligand carrying the populated π^* molecular orbital characterizing the T_1 state (see Figure 10). The analysis of the potential energy surface (PES) near the optimized T_1 geometries shows that the triplet excited state PES is much shallower than the ground state

dx.doi.org/10.1021/ic2011474 | *Inorg. Chem.* 2012, 51, 799−811

PES, and therefore a distortion of the ppy ligands along the δ_i angles can have an important contribution for the tuning of the emission bands (in addition to the chemical substitution discussed previously). Furthermore, this increased ligand flexibility coupled with a larger heavy-atom effect of bromine could possibly open novel nonradiative deactivation channels for **BrIrPic**, as observed experimentally.

CONCLUSION

In summary, a homologous series of bis-cyclometalated iridium(III) complexes Ir(2,4-di-X-phenyl-pyridine)$_2$-(picolinate) (X = H, F, Cl, Br) **HIrPic**, **FIrPic**, **ClIrPic**, and **BrIrPic** has been synthesized and fully characterized. In the present case, a simple variation of the substituent along the halogen group leads to dramatic changes of photophysical properties. Theoretical calculations accurately reproduce the absorption trend for the different halogenated species, provide assignments of the main bands, and confirm the role of SOC in the low energy tail of the absorption spectra. The combined experimental and theoretical results show that Hammett parameters should be separated in σm and σp and their influence on both HOMO and LUMO energy levels should be taken into account for a more accurate and quasi-quantitative assessment of the influence of a substituent on the HOMO−LUMO gap. Furthermore, theoretical results highlight sizable distortions of the populated ppy ligand of the lowest triplet state, which, in combination with the expected heavy atom effect, are likely to play a role in the nonradiative relaxation processes of **BrIrPic**. Overall our results show that the substituents impact the optical properties of the **XIrPic** complexes with both electronic and geometric effects. To be able to understand in detail the impact of the halogen atoms, it is now necessary to separate those two effects, which is the focus of future work.

ASSOCIATED CONTENT

Supporting Information

Absorption and emission spectra in various solvents, additional figures and computational details. This material is available free of charge via the Internet at http://pubs.acs.org.

AUTHOR INFORMATION

Corresponding Author

*E-mail: etienne.baranoff@epfl.ch (E.B.), gianluca.accorsi@isof.cnr.it (G.A.).

ACKNOWLEDGMENTS

We acknowledge financial support for this work by Solvay S.A., the European Union (CELLO, STRP 248043), and the Swiss National Science Fundation (NCCR-MUST interdisciplinary research program), and thank Dr. Davide Di Censo for his kind assistance with electrochemical measurements.

REFERENCES

(1) Armaroli, N.; Balzani, V. *Energy for a Sustainable World: From the Oil Age to a Sun-Powered Future*; Wiley-VCH: Weinheim, Germany, 2010; p 368.
(2) Balzani, V.; Campagna, S. *Photochemistry and Photophysics of Coordination Compounds I*; Springer-Verlag: Heidelberg, Germany, 2007; Vol. *280*.
(3) Balzani, V.; Campagna, S. *Photochemistry and Photophysics of Coordination Compounds II*; Springer-Verlag: Heidelberg, Germany, 2007; Vol. *281*.
(4) Katritzky, A. R.; Kuanar, M.; Slavov, S.; Hall, C. D.; Karelson, M.; Khan, I.; Dobchev, D. A. *Chem. Rev.* **2010**, *110*, 5714.
(5) Verma, R. P.; Hansch, C. *Chem. Rev.* **2011**, *111*, 2865.
(6) Makedonas, C.; Mitsopoulou, C. A. *Eur. J. Inorg. Chem.* **2007**, 4176.
(7) Hansch, C.; Leo, A.; Taft, R. W. *Chem. Rev.* **1991**, *91*, 165.
(8) Hammett, L. P. *Chem. Rev.* **1935**, *17*, 125.
(9) Alexiou, C.; Lever, A. B. P. *Coord. Chem. Rev.* **2001**, *216−217*, 45.
(10) Chen, L. Q.; Yang, C. L.; Li, S. Y.; Qin, J. H. *Spectrochim. Acta, Part A* **2007**, *68*, 317.
(11) McClure, D. S. *J. Chem. Phys.* **1949**, *17*, 905.
(12) Flamigni, L.; Barbieri, A.; Sabatini, C.; Ventura, B.; Barigelletti, F. *Top. Curr. Chem.* **2007**, *281*, 143.
(13) Baranoff, E.; Yum, J. H.; Graetzel, M.; Nazeeruddin, M. K. *J. Organomet. Chem.* **2009**, *694*, 2661.
(14) Chi, Y.; Chou, P. T. *Chem. Soc. Rev.* **2010**, *39*, 638.
(15) You, Y.; Park, S. Y. *Dalton Trans.* **2009**, 1267.
(16) Ulbricht, C.; Beyer, B.; Friebe, C.; Winter, A.; Schubert, U. S. *Adv. Mater.* **2009**, *21*, 4418.
(17) Lowry, M. S.; Hudson, W. R.; Pascal, R. A.; Bernhard, S. *J. Am. Chem. Soc.* **2004**, *126*, 14129.
(18) De Angelis, F.; Fantacci, S.; Evans, N.; Klein, C.; Zakeeruddin, S. M.; Moser, J.-E.; Kalyanasundaram, K.; Bolink, H. J.; Grätzel, M.; Nazeeruddin, M. K. *Inorg. Chem.* **2007**, *46*, 5989.
(19) Bronstein, H. A.; Finlayson, C. E.; Kirov, K. R.; Friend, R. H.; Williams, C. K. *Organometallics* **2008**, *27*, 2980.
(20) Coughlin, F. J.; Westrol, M. S.; Oyler, K. D.; Byrne, N.; Kraml, C.; Zysman-Colman, E.; Lowry, M. S.; Bernhard, S. *Inorg. Chem.* **2008**, *47*, 2039.
(21) Gupta, D.; Katiyar, M.; Deepak.; Hazra, T.; Verma, A.; Marloharan, S. S.; Biswas, A. *Opt. Mater.* **2006**, *28*, 1355.
(22) Xu, M. L.; Zhou, R.; Wang, G. Y.; Xiao, Q.; Du, W. S.; Che, G. B. *Inorg. Chim. Acta* **2008**, *361*, 2407.
(23) Zhang, M.; Li, Z. S.; Li, Y.; Liu, J.; Sun, J. Z. *Int. J. Quantum Chem.* **2009**, *109*, 1167.
(24) Minaev, B.; Minaeva, V.; Agren, H. *J. Phys. Chem. A* **2009**, *113*, 726.
(25) Baranoff, E.; Jung, I.; Scopelliti, R.; Solari, E.; Grätzel, M.; Nazeeruddin, M. K. *Dalton Trans.* **2011**, *40*, 6860.
(26) Holmes, R. J.; Forrest, S. R.; Tung, Y. J.; Kwong, R. C.; Brown, J. J.; Garon, S.; Thompson, M. E. *Appl. Phys. Lett.* **2003**, *82*, 2422.
(27) Sudhakar, M.; Djurovich, P. I.; Hogen-Esch, T. E.; Thompson, M. E. *J. Am. Chem. Soc.* **2003**, *125*, 7796.
(28) Thesen, M. W.; Krueger, H.; Janietz, S.; Wedel, A.; Graf, M. *J. Polym. Sci., Part A: Polym. Chem.* **2010**, *48*, 389.
(29) Jensen, T.; Pedersen, H.; Bang-Andersen, B.; Madsen, R.; Jørgensen, M. *Angew. Chem., Int. Ed.* **2008**, *47*, 888.
(30) Kamei, T.; Fujita, K.; Itami, K.; Yoshida, J.-I. *Org. Lett.* **2005**, *7*, 4725.
(31) Zhao, Y.; Truhlar, D. G. *Theor. Chem. Acc.* **2008**, *120*, 215.
(32) Hay, P. J.; Wadt, W. R. *J. Chem. Phys.* **1985**, *82*, 299.
(33) McLean, A. D.; Chandler, G. S. *J. Chem. Phys.* **1980**, *72*, 5639.
(34) Frisch, M. J.; Trucks, G. W.; Schlegel, H. B.; Scuseria, G. E.; Robb, M. A.; Cheeseman, J. R.; Scalmani, G.; Barone, V.; Mennucci, B.; Petersson, G. A.; Nakatsuji, H.; Caricato, M.; Li, X.; Hratchian, H. P.; Izmaylov, A. F.; Bloino, J.; Zheng, G.; Sonnenberg, J. L.; Hada, M.; Ehara, M.; Toyota, K.; Fukuda, R.; Hasegawa, J.; Ishida, M.; Nakajima, T.; Honda, Y.; Kitao, O.; Nakai, H.; Vreven, T.; Montgomery, J., J. A.; Peralta, J. E.; Ogliaro, F.; Bearpark, M.; Heyd, J. J.; Brothers, E.; Kudin, K. N.; Staroverov, V. N.; Kobayashi, R.; Normand, J.; Raghavachari, K.; Rendell, A.; Burant, J. C.; Iyengar, S. S.; Tomasi, J.; Cossi, M.; Rega, N.; Millam, J. M.; Klene, M.; Knox, J. E.; Cross, J. B.; Bakken, V.; Adamo, C.; Jaramillo, J.; Gomperts, R.; Stratmann, R. E.; Yazyev, O.; Austin, A. J.; Cammi, R.; Pomelli, C.; Ochterski, J. W.; Martin, R. L.; Morokuma, K.; Zakrzewski, V. G.; Voth, G. A.; Salvador, P.; Dannenberg, J. J.; Dapprich, S.; Daniels, A. D.; Farkas, Ö.; Foresman, J. B.; Ortiz, J. V.; Cioslowski, J.; Fox, D. J. *Gaussian 09*, Revision A.02; Gaussian, Inc.: Wallingford, CT, 2009.

(35) Tomasi, J.; Mennucci, B.; Cammi, R. *Chem. Rev.* **2005**, *105*, 2999.
(36) Scalmani, G.; Frisch, M. J.; Mennucci, B.; Tomasi, J.; Cammi, R.; Barone, V. *J. Chem. Phys.* **2006**, *124*, 094107.
(37) te Velde, G.; Bickelhaupt, F. M.; van Gisbergen, S. J. A.; Fonseca Guerra, C.; Baerends, E. J.; Snijders, J. G.; Ziegler, T. *J. Comput. Chem.* **2001**, *22*, 931.
(38) Fonseca Guerra, C.; Snijders, J. G.; te Velde, G.; Baerends, E. J. *Theor. Chem. Acc.* **1998**, *99*, 391.
(39) Wang, F.; Ziegler, T.; van Lenthe, E.; van Gisbergen, S. J. A.; Baerends, E. J. *J. Chem. Phys.* **2005**, *122*, 204103.
(40) Swiderek, K.; Paneth, P. *J. Phys. Org. Chem.* **2009**, *22*, 845.
(41) Zhao, Y.; Schultz, N. E.; Truhlar, D. G. *J. Chem. Theory Comput.* **2006**, *2*, 364.
(42) Demas, J. N.; Crosby, G. A. *J. Phys. Chem.* **1971**, *75*, 991.
(43) Nakamaru, K. *Bull. Chem. Soc. Jpn.* **1982**, *55*, 2697.
(44) *CrysAlis PRO*, 171.34.49; Agilent Technologies: Santa Clara, CA, 2010.
(45) Duisenberg, A. J. M.; Kroon-Batenburg, L. M. J.; Schreurs, A. M. M. *J. Appl. Crystallogr.* **2003**, *36*, 220.
(46) Blessing, R. H. *Acta Crystallogr., Sect. A* **1995**, *51*, 33.
(47) Sheldrick, G. M. *Acta Crystallogr., Sect. A* **2008**, *64*, 112.
(48) Xu, M.-L.; Che, G.-B.; Li, X.-Y.; Xiao, Q. *Acta Crystallogr.* **2009**, *E65*, m28.
(49) Lamansky, S.; Djurovich, P.; Murphy, D.; Abdel-Razzaq, F.; Kwong, R.; Tsyba, I.; Bortz, M.; Mui, B.; Bau, R.; Thompson, M. E. *Inorg. Chem.* **2001**, *40*, 1704.
(50) Schmid, B.; Garces, F. O.; Watts, R. J. *Inorg. Chem.* **1994**, *33*, 9.
(51) Li, J.; Djurovich, P. I.; Alleyne, B. D.; Yousufuddin, M.; Ho, N. N.; Thomas, J. C.; Peters, J. C.; Bau, R.; Thompson, M. E. *Inorg. Chem.* **2005**, *44*, 1713.
(52) Suzuki, K.; Kobayashi, A.; Kaneko, S.; Takehira, K.; Yoshihara, T.; Ishida, H.; Shiina, Y.; Oishic, S.; Tobita, S. *Phys. Chem. Chem. Phys.* **2009**, *11*, 9850.
(53) Ishida, H.; Tobita, S.; Hasegawa, Y.; Katoh, R.; Nozaki, K. *Coord. Chem. Rev.* **2010**, *254*, 2449.
(54) Tsuboyama, A.; Iwawaki, H.; Furugori, M.; Mukaide, T.; Kamatani, J.; Igawa, S.; Moriyama, T.; Miura, S.; Takiguchi, T.; Okada, S.; Hoshino, M.; Ueno, K. *J. Am. Chem. Soc.* **2003**, *125*, 12971.
(55) Orselli, E.; Kottas, G. S.; Konradsson, A. E.; Coppo, P.; Fröhlich, R.; De Cola, L.; van Dijken, A.; Buchel, M.; Börner, H. *Inorg. Chem.* **2007**, *46*, 11082.
(56) Kubin, J.; Testa, A. C. *J. Photochem. Photobiol., A* **1994**, *83*, 91.
(57) Sarkar, A.; Chakravorti, S. *J. Lumin.* **1995**, *65*, 163.
(58) Vlcek, A. A.; Dodsworth, E. S.; Pietro, W. J.; Lever, A. B. P. *Inorg. Chem.* **1995**, *34*, 1906.
(59) Hay, P. J. *J. Phys. Chem. A* **2002**, *106*, 1634.
(60) Lin, C. F.; Huang, W. S.; Chou, H. H.; Lin, J. T. *J. Organomet. Chem.* **2009**, *694*, 2757.
(61) Laskar, I. R.; Chen, T.-M. *Chem. Mater.* **2004**, *16*, 111.
(62) Baranoff, E.; Fantacci, S.; De Angelis, F.; Zhang, X.; Scopelliti, R.; Grätzel, M.; Nazeeruddin, M. K. *Inorg. Chem.* **2011**, *50*, 451.
(63) Casida, M. E. In *Recent Advances in Density-Functional Methods*; World Scientific: Singapore, 1995, 155.
(64) Petersilka, M.; Gossmann, U. J.; Gross, E. K. U. *Phys. Rev. Lett.* **1996**, *76*, 1212.
(65) De Angelis, F.; Belpassi, L.; Fantacci, S. *J. Mol. Struct. Theochem.* **2009**, *914*, 74.
(66) Di Censo, D.; Fantacci, S.; De Angelis, F.; Klein, C.; Evans, N.; Kalyanasundaram, K.; Bolink, H. J.; Gratzel, M.; Nazeeruddin, M. K. *Inorg. Chem.* **2008**, *47*, 980.